Ball-impact energy analysis of wet tumbling mill using a modified discrete element method considering the velocity dependence of friction coefficient

Ball-impact energy analysis of wet tumbling mill using a modified discrete element method considering the velocity dependence of friction coefficient

Tomohiro Iwasaki*, Hiroyuki Yamanouchi

Department of Chemical Engineering, Osaka Prefecture University

1-1 Gakuen-cho, Naka-ku, Sakai, Osaka 599-8531, Japan

* Corresponding author. iwasaki@chemeng.osakafu-u.ac.jp

Abstract

A modified three-dimensional quasi-wet discrete element method (DEM), which is constructed by adding the drag force and buoyancy and the velocity dependence of the friction coefficient of a ball to a conventional dry DEM model, is proposed for analyzing the impact energy of balls in wet ball-milling processes. A comparison of the calculated ball motion in water as the liquid medium with the experimental results demonstrated the validity of the proposed model. The friction coefficient decreased with the increase in the vessel rotational speed and was expressed as a function of the rotational speed and loading amount of the balls. The velocity dependence of the friction coefficient was similar to the variation in the friction coefficient with the sliding velocity, as derived from the lubrication theory. A numerical analysis of the impact energy distribution in the vessel showed that relatively high-impact energies of the balls were intensively generated near the vessel wall, indicating that the wet ball-milling processes were controlled by the impact energy between the ball and the wall. Our model can contribute to reducing the calculation load for simulating the ball motion in wet ball-milling processes compared with the coupling models such as DEM-CFD.

Keywords: Wet milling, DEM, Impact energy, Friction coefficient, Velocity dependence, Lubrication

1. Introduction

Wet ball-milling processes using horizontal tumbling mills have been conventionally employed in various industries, e.g., mining, ceramics, foods, fine chemicals, and pharmaceuticals, owing to their versatility (Danha et al., 2015; Iwasaki et al., 2013; Katou et al., 2019). Mechanical energy, such as compressive and shearing energies, acting on the particulate materials to be treated during wet ball-milling must be precisely controlled to maintain and/or improve the quality and performance of industrial products obtained from the milling processes. It is necessary to determine the impact energy of grinding balls by thoroughly analyzing their motion in the milling vessel to control the mechanical energy. Generally, numerical approaches are often used because experimental investigations of the ball motion are complicated. Among the numerical techniques, the coupling model of computational fluid dynamics (CFD) and discrete element method (DEM), i.e., the Eulerian-Lagrangian approach, is an effective method for analyzing the particle behavior in liquid-solid mixed-phase systems (Al-Arkawazi et al., 2017; Blais and Bertrand, 2017; Blais et al., 2017; Golshan et al., 2020). Some wet ball-milling processes have been analyzed using the CFD-DEM coupling method (Mayank et al., 2015). Although the CFD-DEM method can provide highly accurate numerical data for the ball motion in a fluid flow, the calculation region must be divided into a number of meshes with an appropriate shape and size to obtain valid calculation results, which increases the computational load. Recently, DEM coupled with some particle methods, such as moving particle semi-implicit (MPS) and smoothed particle hydrodynamics (SPH) methods, are also applied in calculating ball motions under wet conditions (Jonsén et al., 2014; Jonsén et al., 2015; Sinnott et al., 2017; Sun et al., 2014). These methods have some advantages that the high-precision calculation can be performed without dividing the calculation region into the meshes and a free surface flow of the fluid can be simulated relatively easily. However, the MPS-DEM and SPH-DEM methods for wet milling processes require a number of small particles expressing the fluid in addition to the balls, which also results in an increase in the computational load. Thus, although the coupling models are effective in analyzing the behavior of both the balls and the fluid during wet milling processes, significant computational efforts are required. Therefore, numerical calculations using the coupling models may be unsuitable for the analysis of practical large-scale processes owing to quite large computational loads (Norouzi et al., 2017).

In most tumbling mills, large and heavy balls are used and are forcefully moved inside the vessel. Consequently, the balls have large inertial forces, which reduce the effects of fluid flow and liquid bridge force on ball motion under wet conditions. Some studies demonstrated that the ball motion in wet milling processes under certain conditions could be numerically analyzed without coupling any fluid flow simulation. Namely, simple quasi-wet DEM models, which are derived from the conventional dry DEM with slight modifications for considering an influence of the fluid on the ball motion, have been proposed. For example, Mori et al. (2004) corrected the external force term in the equation of motion of the dry DEM describing the ball motion with the drag force and buoyancy acting on a single sphere in a stationary fluid. In the model, the frictional force acting on the ball is computed using a constant friction coefficient suitable for wet conditions, which can simulate the experimental average head height of the ball bed during milling. Govender et al. (2013) simulated the ball motion in wet milling using a DEM without considering the drag force and buoyancy by employing a suitable friction coefficient. Although such simple quasi-wet DEMs may not provide strict simulation of wet milling processes compared with the coupling models, the computational load resulted from the fluid flow simulation can be effectively reduced. However, the use of a constant friction coefficient in the models may not adequately simulate the ball motion under wet conditions. This is because the friction coefficient between the solids covered with a liquid can vary, depending on the viscosity of the liquid, the sliding velocity of the solid, and the normal load acting on the solid described using the Stribeck curve according to the lubrication theory (Torbacke et al., 2014).

In this study, a three-dimensional quasi-wet DEM modified by introducing the velocity dependence of the friction coefficient is proposed to describe the ball motion. The distribution of the ball impact energy in a tumbling mill under wet conditions is analyzed using the modified quasi-wet DEM.

2. Calculation and experimental methods

2.1. Calculation

In a quasi-wet DEM, the translational and rotational motions of a ball can be described using the following equations of motion:

$$m\frac{\mathrm{d}^2\boldsymbol{x}}{\mathrm{d}t^2} = \boldsymbol{F}_\mathrm{c} + \boldsymbol{F}_\mathrm{d} + \boldsymbol{F}_\mathrm{b} + m\boldsymbol{g} \quad (1)$$

$$I\frac{\mathrm{d}\boldsymbol{\omega}}{\mathrm{d}t} = \boldsymbol{T} \quad (2)$$

where m, $\boldsymbol{x}$, t, and $\boldsymbol{g}$ are the mass of the ball, the coordinates of the center of the ball, the time, and the gravitational acceleration, respectively. $\boldsymbol{F}_\mathrm{c}$, $\boldsymbol{F}_\mathrm{d}$ and $\boldsymbol{F}_\mathrm{b}$ represent the contact force, drag force and buoyancy acting on the ball, respectively. I, $\boldsymbol{\omega}$, and $\boldsymbol{T}$ denote the moment of inertia, angular velocity, and moment of the ball, respectively. $\boldsymbol{F}_\mathrm{c}$ was expressed by the Hertz-Mindlin contact model. In general, the drag force for a particle is greatly affected by the volume fraction of particles in the fluid. However, when both density and size of a particle are quite large like grinding ball, a high inertia force can act on the particle, which may decrease relatively the influence of volume fraction on the drag force. Therefore, it can be assumed that $\boldsymbol{F}_d$ is approximated by the drag force acting on a single sphere in a stationary fluid, according to the wet DEM model proposed by Mori et al. (2004). Thus, $\boldsymbol{F}_d$ and $\boldsymbol{F}_b$ can be expressed using Eqs. (3) and (4), respectively:

$$\boldsymbol{F}_{\mathrm{d}} = -\frac{1}{2}(C_{\mathrm{D}} A\rho|\boldsymbol{v}|)\boldsymbol{v} \quad (3)$$

$$\boldsymbol{F}_{\mathrm{b}} = -V\rho\boldsymbol{g} \quad (4)$$

where ρ is the density of fluid, and A, $\boldsymbol{v}$, and V are the projected area, translational velocity, and volume of the ball, respectively. C_D is the drag coefficient and can be calculated using Eqs. (5)–(7), in accordance with the particle Reynolds number Re_p of the ball.

$$C_D = 24/\mathrm{Re}_p \quad \text{at } \mathrm{Re}_p < 1 \quad (5)$$

$$C_D = (0.55 + 4.8/\mathrm{Re}_p^{0.5})^2 \quad \text{at } 1 < \mathrm{Re}_p < 10^4 \quad (6)$$

$$C_D = 0.44 \quad \text{at } \mathrm{Re}_p > 10^4 \quad (7)$$

The conventional DEM considers the sliding and rolling frictions for calculating the contact force and moment of a particle. The rolling friction is influenced by the surface roughness and cohesiveness of the contact solid; however, when the liquid lies between solids, such as when the balls collide in a medium, the rolling friction of the solids significantly decreases owing to lubrication (Butt et al., 2003). Accordingly, during the wet ball-milling processes, the effect of the rolling friction of balls on the wet ball-milling behavior may be small. Therefore, the rolling friction may be neglected in this analysis, but the sliding friction plays a critical role. In this study, the effect of sliding friction on the ball movement was the main focus.

When analyzing the mechanical energy generated during wet ball-milling, the impact energy E_i of the ball during a single collision (Kano and Saito, 1998) and the accumulated value of E_i per second, E, are calculated using by Eqs. (8) and (9), respectively:

$$E_i = (1/2)mv_{ij}^2 \tag{8}$$

$$E = \sum^{N} E_i \tag{9}$$

where i and j are the numbers of the contacting balls, v_{ij} is the relative velocity of the ball just before the collision, and N is the number of collisions per second.

The ball behavior was simulated in three dimensions using the parameters listed in Table 1, corresponding to the experimental set up and operating conditions to be discussed later. A schematic of the horizontal tumbling ball mill was illustrated in Fig. 1. The milling vessel has no lifters; the interior surface of vessel is smooth. The coefficients of restitution were experimentally determined. Assuming that the surface properties of ball and vessel wall hardly affect the amount of friction between fully wetted surfaces due to the presence of a relatively thick liquid film on the surfaces, the friction coefficients between balls and between the ball and wall were identical (Mori et al., 2004) and were varied in the simulation. Under the loading amount of the liquid medium used in this study, most of the balls were submerged during milling. It was assumed that both the drag force and the buoyancy always acted on all the balls. The motions of the balls near the milling vessel cap were determined; the balls of which the central coordinate was within 12 mm from the cap were detected to match the experimental measurement. The calculated values were compared with the experimental ones. In the calculation, a short time step (0.1 μsec) was used to avoid divergence of the computations using the stiffness of ball and wall determined respectively with the actual Young's moduli of alumina (aluminum oxide, Al_2O_3) and PTFE. The computational load in the simulation was relatively small even when using the short time step, compared with the coupling models; for example, when using a desktop computer with Intel Core i7 (4.2 GHz) processor, each calculation was completed within a few days.

2.2. Experimental methods

In the experimental investigations of the ball motion, a cylindrical vessel with an inner diameter of 90 mm and a depth of 80 mm and Al_2O_3 balls of 10 mm diameter were used, which was similar to Fig. 1. The vessel was made of stainless steel, and the inner part was coated with PTFE. No lifters were equipped. The experimental conditions are listed in Table 2. The values of the ball loading J, defined as the ratio of the bulk volume of the ball bed (including the voids among the balls) to the vessel capacity, were 0.4 and 0.5. The void fraction of the ball beds under static conditions was 0.39, regardless of the value of J. Deionized water was used as the medium. The water loading, defined as the ratio of the total actual volumes of both water and balls to the vessel capacity, was maintained at 0.7; the loading amounts of water were 233 and 202 g for $J = 0.4$ and 0.5, respectively. The critical rotational speed ratio φ of the vessel, defined as the ratio of the operating speed n to the ideal critical speed n_c (= 2.35 s^{-1}), i.e., $\varphi = n/n_c$, which was determined as $n_c = (2g/D)^{0.5}/(2\pi)$ (g: gravity acceleration, D: vessel diameter) from the equilibrium of gravity and centrifugal force acting on a ball. In this work, φ was varied from 0.3 to 1.3 in which a continuous circulating flow of balls is formed in the vessel.

The steady-state motion of the balls in the vessel was directly observed from outside to verify the validity of our model through a transparent plastic lid, using a digital camera at a frame rate of 399.3 fps. The captured images were analyzed using image-processing software (ImageJ with TrackMate) to detect the position of the balls near the lid at a given time and to determine the velocity of each ball (Broeke et al., 2015; Tinevez et al., 2017). The average head height of the balls and the velocity distribution in the vessel were obtained using the determined experimental ball motion and compared with those of the simulation.

3. Results and discussion

3.1. Velocity dependence of friction coefficient

Fig. 2 shows the variation in the average head height (calculated using various friction coefficients) with the critical rotational speed ratio φ for both calculated and experimental data. The experimental average head height at $J = 0.4$ was almost constant regardless of the φ value. However, the experimental average head height at $J = 0.5$ slightly increased with φ owing to an increase in the frictional force between the ball and the vessel wall with increasing normal stress acting on the balls in contact with the vessel wall. In contrast, the calculated average head height significantly increased with φ for both J values. Furthermore, for each J value, when a constant friction coefficient was used in the calculation, the variations in the experimental and calculated average head heights with φ were no consistent with each other. The results suggest that the friction coefficient varied depending on φ. Therefore, the friction coefficient in which the experimental average head height agreed with the calculated value was determined at each φ. Fig. 3 shows the variation of the adjusted friction coefficient μ_a with φ for each J value. The velocity dependence of μ_a was confirmed; μ_a decreased with an increase in φ, indicating the lubricating effect of water. Fig. 4 confirms that the average head heights calculated using μ_a well coincide with the experimental data, which suggests that μ_a is valid.

According to the lubrication theory (Torbacke et al., 2014), the variation in the friction coefficient with the operating conditions can be described using the Stribeck curve as a parameter of $\eta v_s/F$. In the above expression, η is the viscosity of the liquid, v_s is the relative sliding velocity between solids, and F is the normal load. Therefore, assuming that η is constant and that v_s and F in the wet ball-milling are proportional to φ and J, respectively, the adjusted friction coefficient μ_a was analyzed using the parameter φ/J, which correspond to $\eta v_s/F$. As shown in Fig. 5, μ_a decreases monotonically with increasing φ/J, as expressed using Eq. (10). This variation tendency may correspond to that in the mixed lubrication region of the Stribeck curve (Torbacke et al., 2014).

$$\mu_a = 0.31(\varphi/J)^{-0.40} \tag{10}$$

Using the adjusted friction coefficient suitable for the critical rotational speed ratio and the ball loading ratio determined using Eq. (10), the ball movement was calculated for each J value, and the 3-sec averaged velocity distribution of the balls was determined and compared with those of the experimental results. Furthermore, the absolute errors of velocity and moving direction of balls between the experimental data and the calculated values were computed. The absolute error of the direction was defined as the angle between the experimental and calculated velocity vectors. As shown in Fig. 6, except for the center of ball beds in which the ball motion could be quite slow and irregular (random), the absolute errors were small under the given conditions, indicating that the calculation results almost agreed with the experimental values at each φ. These findings demonstrate that our model considering the velocity dependence of μ_a can satisfactorily express the actual motion of balls in wet milling.

3.2. Impact energy analysis

Fig. 7a shows the accumulated impact energy E, with its normal and tangential components, E_n and E_t, using J = 0.5 as an example. E was approximately proportional to the square of φ, indicating that E corresponds to the rotational energy of the vessel. In addition, E significantly depended on E_t rather than E_n. The impact energy was analyzed by dividing E into two parts, i.e., E_b and E_w, representing the accumulated impact energies between the balls, and between the ball and the wall, respectively. As shown in Fig. 7b, E_w exponentially increased with φ, whereas E_b was linearly proportional to φ. The results imply that the dependence of E on φ was significantly influenced by E_w in comparison with E_b. The frequency distribution of E in the vessel at each φ value was computed to analyze the variation in E_w with φ. Fig. 8 shows the 3-sec averaged energy-basis and number-basis frequency distributions at J = 0.5. In both distributions, high-frequency values were observed along the vessel wall as φ increased. As shown in Fig. 6, the motion of balls near the vessel wall was relatively gentle because they moved together like a rigid body, which induced the reduction of impact energy between the balls. In contrast, the ball-to-wall relative velocity was large due to sliding and a large amount of the impact energy generated, according to the definition of impact energy by Eq. (8). Therefore, large impact energies tended to generate within the region between the slowly moving assembly of balls and the fast moving wall (i.e., the shear zone). Consequently, wet ball-milling processes may be controlled through the impact energy of the balls in contact with the vessel wall.

4. Conclusions

A modified quasi-wet DEM considering the vessel speed dependence of the friction coefficient of a ball is proposed. The validity of this method was demonstrated through a comparison of the calculation results of the ball motion in a milling vessel with the experimental results. The velocity dependence of the friction coefficient was similar to the variation in the friction coefficient with the sliding velocity, as described using the lubrication theory. Our model can contribute to the reduction of calculation loads in simulating ball motion in wet milling processes. The numerical analysis of the ball-impact energy showed that relatively high-impact energy of balls was intensively generated near the vessel wall, indicating that wet ball-milling processes are controlled by the impact energy between the ball and the wall. According to the lubrication theory, the friction coefficient should be varied depending on the normal load acting on the ball. Thus, apart from the effects of operating conditions such as ball loading and ball diameter, the effects of the normal load dependence on the ball motion under wet conditions should be investigated in detail.

Nomenclature

A	Projected area of the ball (m^2)
C_D	Drag coefficient (–)
D	Vessel diameter (m)
E	Accumulated impact energy (J/s)
E_n	Normal components of E (J/s)
E_t	Tangential component of E (J/s)
E_b	Accumulated impact energy between balls (J/s)
E_w	Accumulated impact energy between the ball and the wall (J/s)
E_i	Impact energy of the ball at single collision (J)
F	Normal load (N)
$\boldsymbol{F}_c$	Contact force (N)
$\boldsymbol{F}_d$	Drag force (N)
$\boldsymbol{F}_b$	Buoyancy (N)
$\boldsymbol{g}$	Gravity acceleration (m/s^2)
I	Moment of inertia of ball ($kg\cdot m^2$)
J	Ball loading volume ratio (–)
m	Mass of the ball (kg)

$\boldsymbol{N}$ Number of collisions per unit time (s^{-1})

$\boldsymbol{n}$ Vessel speed (s^{-1})

$\boldsymbol{n}_c$ Ideal critical vessel speed (s^{-1})

Re_p Particle Reynolds number of the ball (–)

$\boldsymbol{T}$ Moment of the ball (N·m)

$\boldsymbol{t}$ Time (s)

$\boldsymbol{V}$ Volume of the ball (m^3)

$\boldsymbol{v}$ Translational velocity of ball (m/s)

v_{ij} Relative velocity of the ball just before the collision (m/s)

v_s Relative sliding velocity between solids (m/s)

$\boldsymbol{x}$ Coordinates of the center of the ball (m)

η Viscosity of liquid (Pa·s)

μ_a Adjusted friction coefficient (–)

ρ Density of fluid (kg/m^3)

φ Critical rotational speed ratio (–)

$\boldsymbol{\omega}$ Angular displacement of the ball (rad)

References

Al-Arkawazi, S., Marie, C., Benhabib, K., Coorevits, P., 2017. Modeling the hydrodynamic forces between fluid–granular medium by coupling DEM–CFD. Chem. Eng. Res. Des. 117, 439-447.

Blais, B., Bertrand, F., 2017. CFD-DEM investigation of viscous solid–liquid mixing: impact of particle properties and mixer characteristics. Chem. Eng. Res. Des. 118, 270-285.

Blais, B., Bertrand, O., Fradette, L., Bertrand, F., 2017. CFD-DEM simulations of early turbulent solid–liquid mixing: prediction of suspension curve and just-suspended speed. Chem. Eng. Res. Des. 123, 388-406.

Broeke, J., Mateos Pérez, J.M., Pascau, J., 2015. Image Processing with ImageJ: Extract and Analyze Data from Complex Images with ImageJ, second ed. Packt Publishing, Birmingham.

Butt, H.-J., Graf, K., Kappl, M., 2003. Physics and Chemistry of Interfaces, Wiley-VCH, Weinheim.

Callister, Jr., W.D., Rethwisch, D.G., 2009. Materials Science and Engineering: An Introduction, eighth ed., John Wiley & Sons, Hoboken.

Danha, G., Hildebrandt, D., Glasser, D., Bhondayi, C., 2015. A laboratory scale application of the attainable region technique on a platinum ore. Powder Technol. 274, 14-19.

Golshan, S., Sotudeh-Gharebagh, R., Zarghami, R, Mostoufi, N., Blais, B., Kuipers, J.A.M., 2020. Review and implementation of CFD-DEM applied to chemical process systems. Chem. Eng. Sci. 221, 115646.

Govender, I., Cleary, P.W., Mainza, A.N., 2013. Comparisons of PEPT derived charge features in wet milling environments with a friction-adjusted DEM model. Chem. Eng. Sci. 97, 162–175.

Iwasaki, T., Sato, N., Nakamura, H., Watano, S., 2013. An experimental investigation of aqueous-phase synthesis of magnetite nanoparticles via mechanochemical reduction of goethite. Adv. Powder Technol. 24, 482-486.

Jonsén, P., Pålsson, B.I., Stener, J.F., Häggblad, H.-Å., 2014. A novel method for modelling of interactions between pulp, charge and mill structure in tumbling mills. Miner. Eng. 63, 65-72.

Jonsén, P., Stener, J.F., Pålsson, B.I., Häggblad, H., 2015. Validation of a model for physical interactions between pulp, charge and mill structure in tumbling mills. Miner. Eng. 73, 77–84.

Kano, J., Saito, F., 1998. Correlation of powder characteristics of talc during planetary ball milling with the impact energy of the balls simulated by the particle element method. Powder Technol. 98, 166–170.

Katou, K., Shimojima, K., Hosokawa, H., 2019. Preparation for $WCNi_3Al$ hard metal by vacuum sintering. Mater. Trans. 60, 471-475.

Mayank, K., Malahe, M., Govender, I., Mangadoddy, N., 2015. Coupled DEM-CFD model to predict the tumbling mill dynamics. Procedia IUTAM 15, 139–149.

Mori, H., Mio, H., Kano, J., Saito, F., 2004. Ball mill simulation in wet grinding using a tumbling mill and its correlation to grinding rate. Powder Technol. 143–144, 230–239.

Norouzi, H.R., Zarghami, R., Mostoufi, N., 2017. New hybrid CPU-GPU solver for CFD-DEM simulation of fluidized beds. Powder Technol. 316, 233–244.

Sinnott, M.D., Cleary, P.W., Morrison, R.D., 2017. Combined DEM and SPH simulation of overflow ball mill discharge and trommel flow. Miner. Eng. 108, 93–108.

Sun, X., Sakai, M., Sakai, M., Yamada, Y., 2014. A Lagrangian–Lagrangian coupled method for three-dimensional solid–liquid flows involving free surfaces in a rotating cylindrical tank. Chem. Eng. J. 246, 122–141.

Tinevez, J.-Y., Perry, N., Schindelin, J., Hoopes, G.M., Reynolds, G.D., Laplantine, E., Bednarek, S.Y., Shorte, S.L., Eliceiri, K.W., 2017. TrackMate: an open and extensible platform for single-particle tracking. Methods 115, 80–90.

Torbacke, M., Rudolphi, Å.K., Kassfeldt, E., 2014. Lubricants: Introduction to Properties and Performance, John Wiley & Sons, Chichester.

Table 1 – Calculation parameters.

Ball material	Alumina (Al_2O_3)
Wall material	Polytetrafluoroethylene (PTFE)
Ball diameter	10 mm
Vessel internal diameter	90 mm
Vessel internal depth	80 mm
Ball loading volume ratio, *J*	0.4, 0.5
Number of balls corresponding to *J*	237, 296
Ball density*	3980 kg/m^3
Young's modulus of ball*	380 GPa
Poisson's ratio of ball*	0.22
Young's modulus of wall*	0.40 GPa
Poisson's ratio of wall*	0.46
Restitution coefficient of ball-to-ball	0.78
Restitution coefficient of ball-to-wall	0.83
Critical rotational speed ratio, φ	0.3, 0.7, 1.0, 1.3
Water density	1000 kg/m^3
Water viscosity	1.0 mPa·s
Time step	0.1 μs
Recording interval of ball coordinates	2.5 ms
Recording time	3.0 s

* Callister and Rethwisch (2009)

Table 2 – Experimental conditions of wet tumbling mill.

Ball material	Al_2O_3
Internal wall material	PTFE
Ball diameter	10 mm
Vessel volume	510 mL
Vessel internal diameter	90 mm
Vessel internal depth	80 mm
Ball filling ratio, *J*	0.4, 0.5
Number of balls corresponding to *J*	237, 296
Porosity of ball bed	0.39
Critical rotational speed ratio, φ	0.3, 0.7, 1.0, 1.3
Frame interval	2.5 ms
Recording time	3.0 s

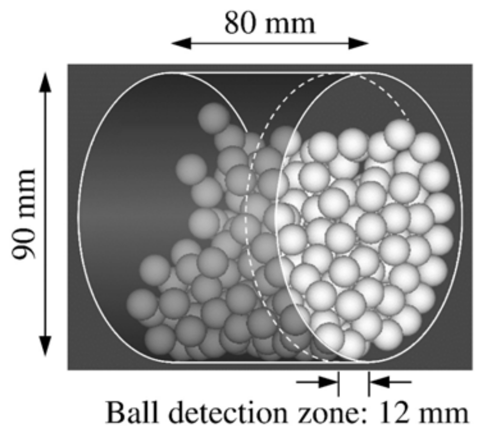

Fig. 1 – Schematic of the horizontal tumbling ball mill.

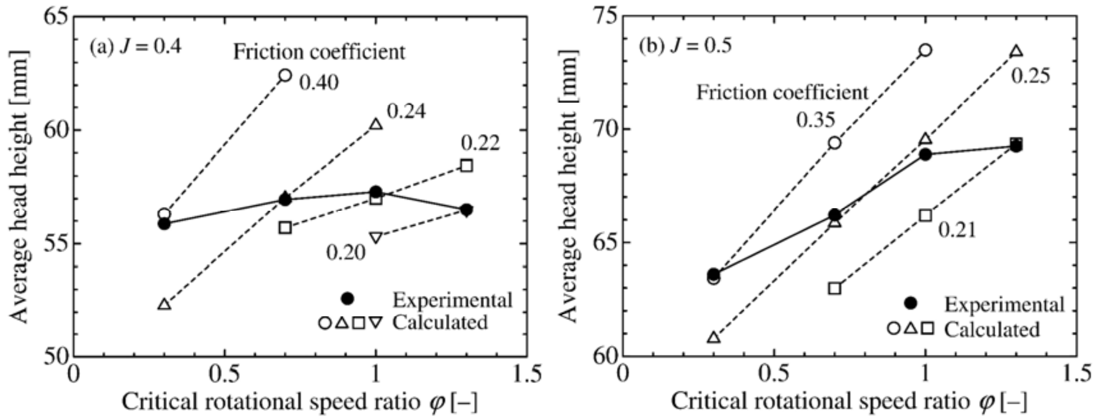

Fig. 2 – Variations in experimental and calculated average head heights with critical rotational speed ratio at J = (a) 0.4 and (b) 0.5.

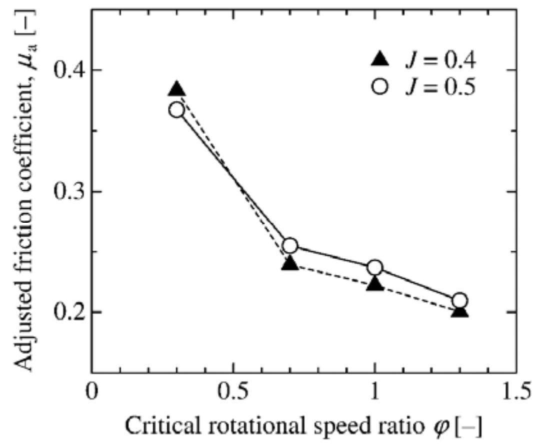

Fig. 3 – Variation in adjusted friction coefficient μ_a with critical rotational speed ratio φ.

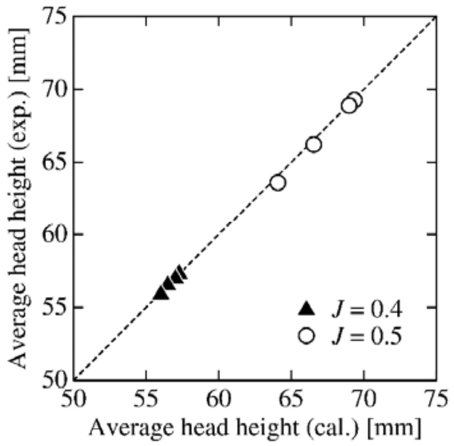

Fig. 4 – Comparison of average head heights calculated with adjusted friction coefficient μ_a with experimental data.

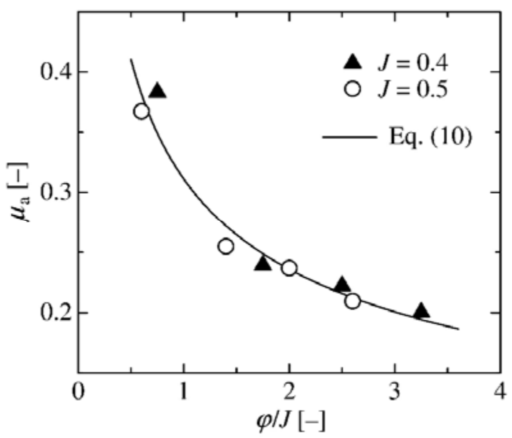

Fig. 5 – Adjusted friction coefficient μ_a as a function of φ/J.

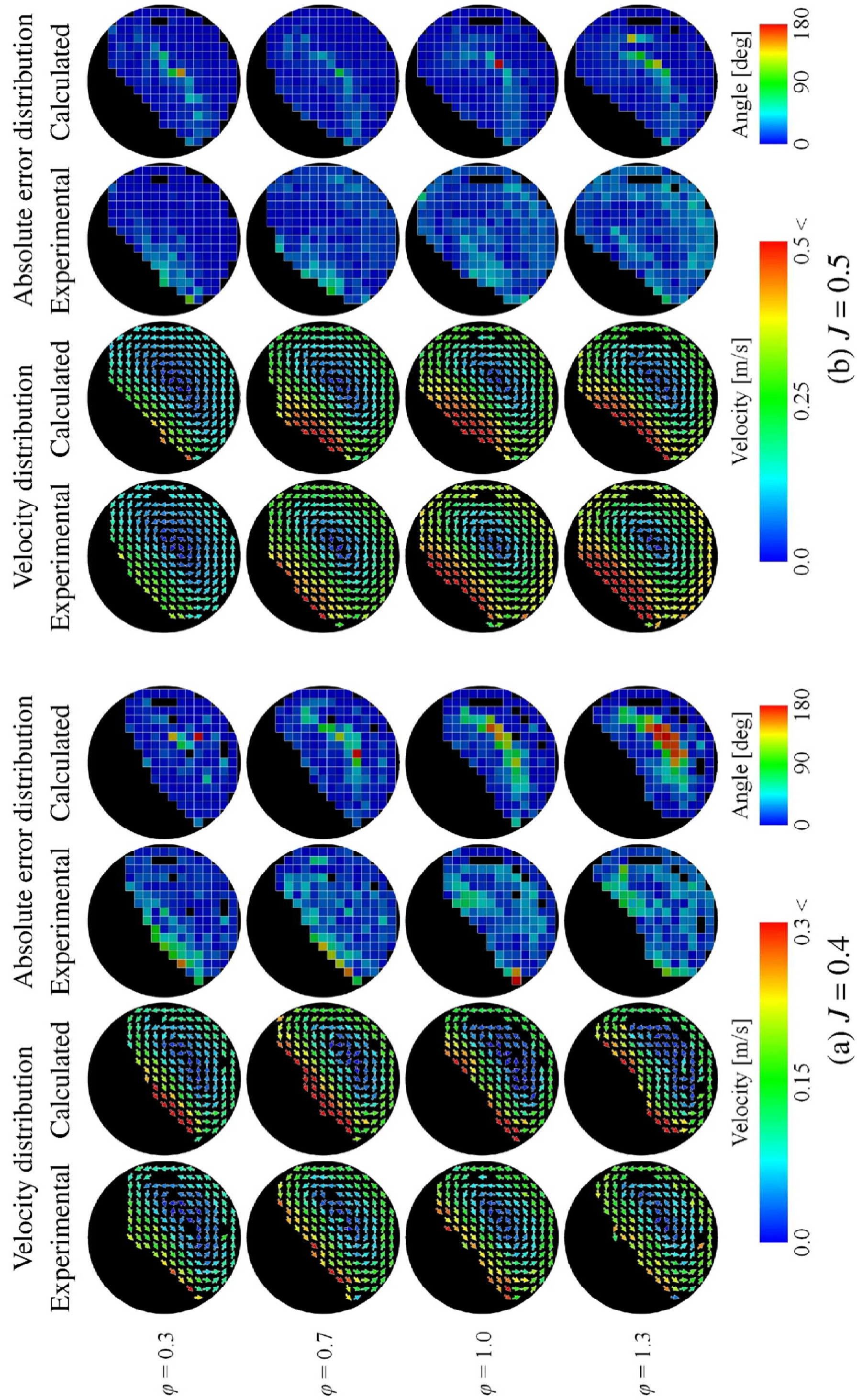

Fig. 6 – Velocity and error distributions at J = 0.4 and 0.5.

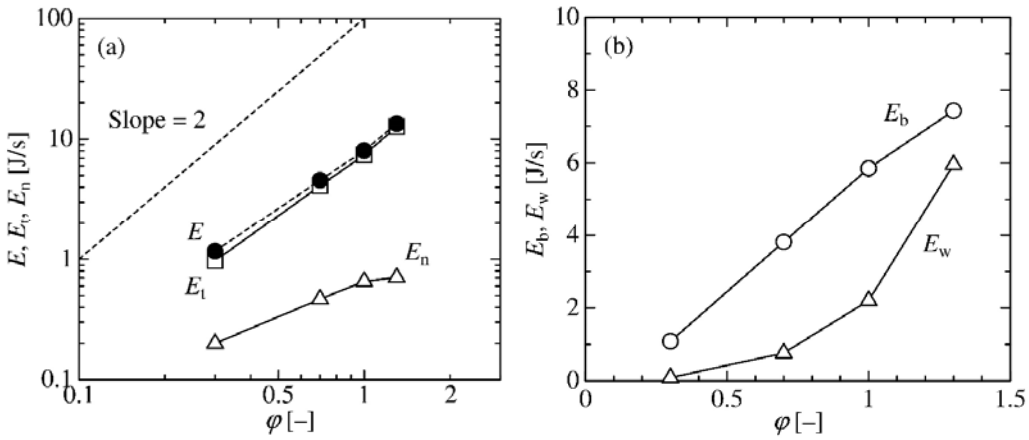

Fig. 7 – Variations in (a) accumulated impact energy and its normal and tangential components and (b) accumulated energy of ball-to-ball and ball-to-wall impacts with critical rotational speed ratio at J = 0.5.

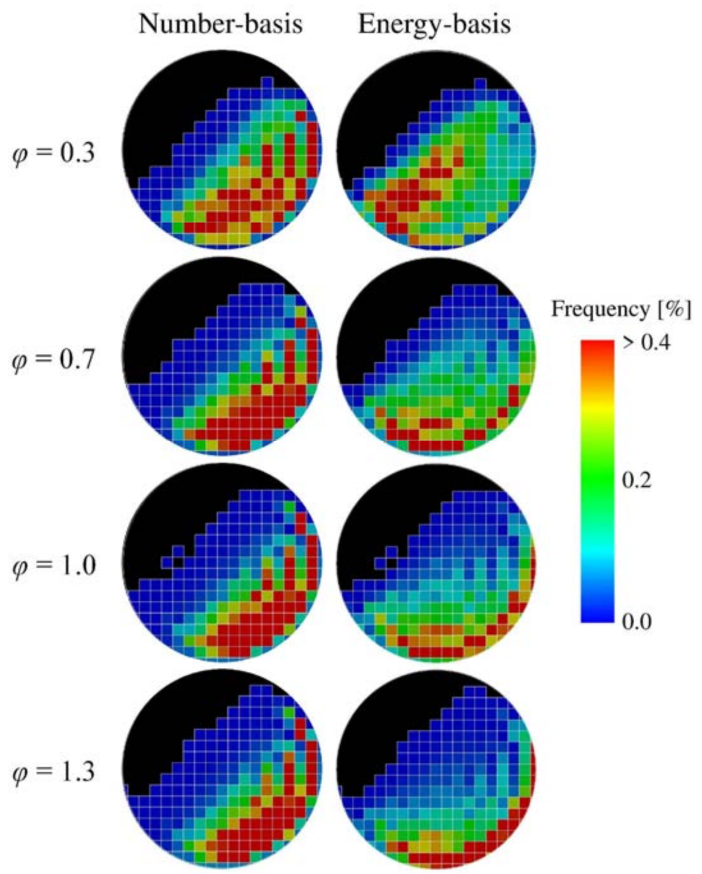

Fig. 8 – Effect of critical rotational speed ratio on the energy-basis and number-basis frequency distributions of impact energy E_w at J = 0.5.